Lawrence Berkeley National Laboratory
LBL Publications

Title
Deciphering helix assembly in the heliconical nematic phase via tender resonant X-ray scattering

Permalink
https://escholarship.org/uc/item/73v0t0gj

Journal
Journal of Materials Chemistry C, 9(31)

ISSN
2050-7526

Authors
Cao, Yu
Feng, Jun
Nallapaneni, Asritha
et al.

Publication Date
2021-08-12

DOI
10.1039/d1tc02027g

Peer reviewed

eScholarship.org Powered by the California Digital Library
University of California

Molecular Packing in Double Gyroid Cubic Phases Revealed *via* Resonant Soft X-ray Scattering

Yu Cao[1,2], Mohamed Alaasar[3,4], Asritha Nallapaneni[2,5], Mirosław Salamończyk[2,6], Peter Marinko[7], Ewa Gorecka[6], Carsten Tschierske[4], Feng Liu[1,*], Nataša Vaupotič[7,8,†], Chenhui Zhu[2,‡]

[1] State Key Laboratory for Mechanical Behavior of Materials, Shaanxi International Research Center for Soft Matter, School of Materials Science and Engineering, Xi'an Jiaotong University, Xi'an 710049, P. R. China

[2] Advanced Light Source, Lawrence Berkeley National Laboratory, Berkeley, CA 94720 USA

[3] Department of Chemistry, Faculty of Science, Cairo University, Giza, Egypt

[4] Institute of Chemistry, Martin-Luther-University Halle-Wittenberg, D-06120 Halle, Germany

[5] Department of Polymer Engineering, University of Akron, Akron, OH 44325 USA

[6] Faculty of Chemistry, University of Warsaw, Zwirki i Wigury 101, 02-089 Warsaw, Poland

[7] Department of Physics, Faculty of Natural Sciences and Mathematics, University of Maribor, Koroška 160, 2000 Maribor, Slovenia

[8] Jozef Stefan Institute, Jamova 39, 1000 Ljubljana, Slovenia

Abstract

The bicontinuous double gyroid phase is one of the nature's most symmetric and complex structures, the electron density map of which was established long ago. By utilizing small-angle X-ray scattering (SAXS), resonant soft X-ray scattering (RSoXS) at the carbon K-edge and model-dependent tensor based scattering theory, we have not only elucidated morphology but also identified molecular packing in the double

gyroid phases formed by molecules with different shapes, i.e. rod-like *vs* taper-shaped, thus validating some of the hypothetical packing models and disapproving others. The spatial variation of molecular orientation through the channel junctions in the double gyroid phase can be either continuous in the case of anisotropic channels or discontinuous in the case of isotropic channels depending on the molecular structure and shape.

To understand self-assembled hierarchical structures in soft matter and biomaterials and to realize their potential in many industrially-relevant areas, there is a high demand for going beyond reconstructed electron density maps or morphology, which is accessible now with existing experimental and theoretical capabilities, and going down in length scale, i.e. deciphering local molecular orbital, chemical bond or molecular level packing in complex structures, which play a key role in the observed microscopic or macroscopic chiral phenomena in soft and biomaterials. The cubic phase in liquid crystal was first discovered by V. Luzzati in 1968 [1] and different types of cubic phases were studied [2-4] since then including the micellar type, which is composed of discrete objects arranged into a cubic lattice [5-8] and the type with continuous network of channels, for example, with $Ia\bar{3}d$ or $Im\bar{3}m$ symmetry, intersected by infinite periodic minimal surfaces [9]: Schoen Gyroid G or Schwarz P, respectively [10-13]. Continuous network phases garnered significant attention due to their complexity and various applications including ion transportation, catalysis, drug delivery, organic electronic devices and energy conversion [14-19].

Among the continuous network phases, a double gyroid $Ia\bar{3}d$ phase is the most common one. The $Ia\bar{3}d$ phase exists in chemically distinct systems including amphiphiles [20,21], polycatenar molecules[11, 22] and polymers [23]. The electron density maps reconstructed from the small-angle X-ray scattering (SAXS) suggest that the double network of channels possess opposite chirality with each network composed of short straight fragments (channels) connected *via* three-way junctions

[24]. While periodic minimal surfaces capture the continuous network structure in mathematical framework reasonably well [25], the chirality of the networks and the fundamental driving force for such symmetry breaking phenomena remains still intriguing. In particular, how molecules are packed in the channels continues to be a longstanding open question. Several packing models have been proposed based on the molecular shape and size [12,26] but there has been no direct validation of these hypotheses on the level of molecular orientation variation until now.

During the past few decades, resonant X-ray scattering based on the anisotropic polarizability of atoms close to their absorption edge has been developed into a powerful characterization tool to probe both the spatial modulations and electronic structure in complex materials [27-30]. Often, sulfur, selenium or chlorine atoms are built into the molecular structure to serve as resonant centers. Recently, resonant soft X-ray scattering (RSoXS) at carbon K-edge enabled significant advancements in probing the *in situ* helical pitch variation [31,32] of B4 helical nanofilaments and the newly discovered twist bend nematic, phase separation in block-copolymers and organic photovoltaic solar cells [33,34]. Close to the absorption edge, the scattering form factor of the resonant atom becomes a complex 2^{nd} order (3×3) tensor, the elements of which are extremely sensitive to the X-ray energy and the bond orientation with respect to the incident and scattered X-ray polarization. Because of this, RSoXS can be used to probe bond orientation ordering of specific bonds, e.g. C-, N-, O-related, which is of great interest especially in the field of organic materials. Using RSoXS, one may observe signals forbidden by the crystallography extinction rule (purely resonant or "forbidden" peaks), which contain highly desirable information on molecular packing. Understanding such forbidden peaks in one-dimensional model structures has been demonstrated in B4 helical nanofilaments and twist bend nematic. However, there has been very limited success in understanding the molecular-level packing in three-dimensional complex phases besides the blue phase.

In this letter, we examined the structure and molecular packing in a double gyroid bicontinuous cubic phase of liquid crystals. Scattering peaks forbidden by the crystallography extinction rules were observed in RSoXS in addition to those observed in SAXS. A combination of SAXS, RSoXS and model-dependent tensor-based scattering pattern simulations enabled validation of two molecular packing models, i.e., continuous and discontinuous at three-way junctions of channels among several previously proposed models.

For these studies, three compounds that differ in molecular structure were chosen (Fig. 1) and all of them form a double gyroid cubic phase. In this work, we focus primarily on the double gyroid cubic phase, however, the same approach can be applied to other phases as well such as the tri-continuous cubic phases. Compound 1 is a rodlike polycatenar molecule (having multiple terminal chains) exhibiting a double gyroid phase $Ia\bar{3}d$ in a temperature range between the isotropic and tetragonal phase. Similar materials were studied before and hypothesized to have a helical molecular packing along the channels [11,22,35,36]. This new compound was synthesized using similar procedures as reported previously [35]. To examine the differences in molecular packing between distinct molecular shapes, we selected two taper-shaped amphiphiles that were systematically investigated in previous studies [20,21].

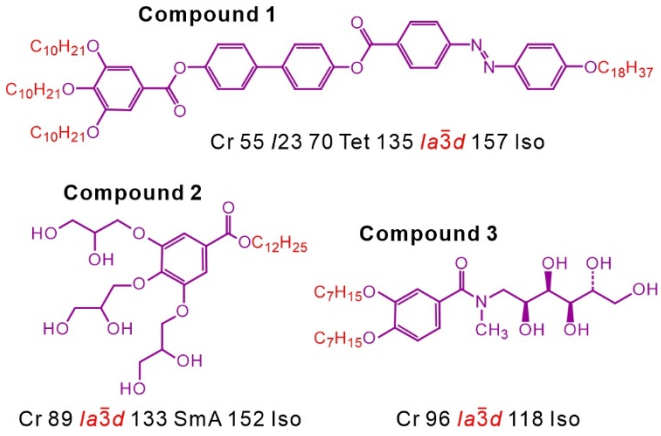

FIG.1. Molecular structures of the studied compounds and phase transition temperatures [20,21]. The purple and red parts of molecules match with the regions of higher and lower electron density on the electron density maps in FIG. 3 and coincide with the polar and nonpolar molecular parts, respectively.

SAXS experiments were conducted at beamline 7.3.3 (10 KeV) at Advanced Light Source (ALS) and beamline BL16B1 (12 KeV) at Shanghai Synchrotron Radiation Facility (SSRF). For all materials, SAXS results (FIG. S1) show several sharp peaks, the positions of which in the scattering vector (q) space are in the ratio of √6: √8: √14: √16: √22: √24, which is consistent with a double gyroid phase. The first two peaks, the strongest reflections in SAXS, are indexed by Miller indices (hkl) as (211) and (220). These are the first two peaks allowed by the extinction rules, without considering resonance effect. Detailed results (unit cell parameter a_{cub}, crystallographic plane spacing or d-spacing for different peaks and their intensities I) are listed in Tables S.I-S.III of the Supplementary Information.

RSoXS was conducted at beamline 11.0.1.2 at ALS. The RSoXS patterns for compounds 1 and 2 at C K-edge (284 eV) are shown in FIGs. 2a, b and S2, S3. Unlike SAXS, the RSoXS results are qualitatively different among the three studied compounds. For compound 1, the peak observed in Fig. S2d corresponds to a d-spacing of 4.69 nm, which is the same as the (211) peak observed in the hard X-ray SAXS (see Tables S.I and S.IV). Hence, the (211) peak is not forbidden and is observable both in hard X-ray SAXS and RSoXS. Using the (211) peak as a reference, the other two resonant peaks were indexed as (110) and (200) respectively (FIGs. 2a and S2). For compound 2, the non-resonant (211) peak is too large in q and out of the accessible q range for RSoXS. Nevertheless, one resonant peak was observed (FIGs. 2b and S3), and indexed as the (110) peak, which gives the lattice parameter a_{cub} = 9.14 nm. Interestingly, no (200) resonant peak was observed. For compound 3, no resonant peak was detected within the same q range. Additional details are provided in FIG. S2-S3 (diffractograms) and Tables S.I-S.V (lattice parameter a_{cub}, d-spacing and intensities) in the Supplementary Information. We note here that the small discrepancy in lattice parameters between SAXS and RSoXS is attributed to the differences associated with sample preparation (1 mm sample thickness in SAXS vs ~1 micron in RSoXS), and the challenges with temperature calibration in RSoXS due to its vacuum

environment and delicate silicon nitride membranes.

In order to verify the resonant character of the signals, X-ray energy scans were conducted from 270 to 290 eV in a step of 0.5 eV for compound 1 (FIG. 2c). The (110) and (200) peaks are strongly dependent on the X-ray energy, which is characteristic of a resonant peak. Similar energy dependence was observed for the (110) peak observed in compound 2 (FIG. S3) as well.

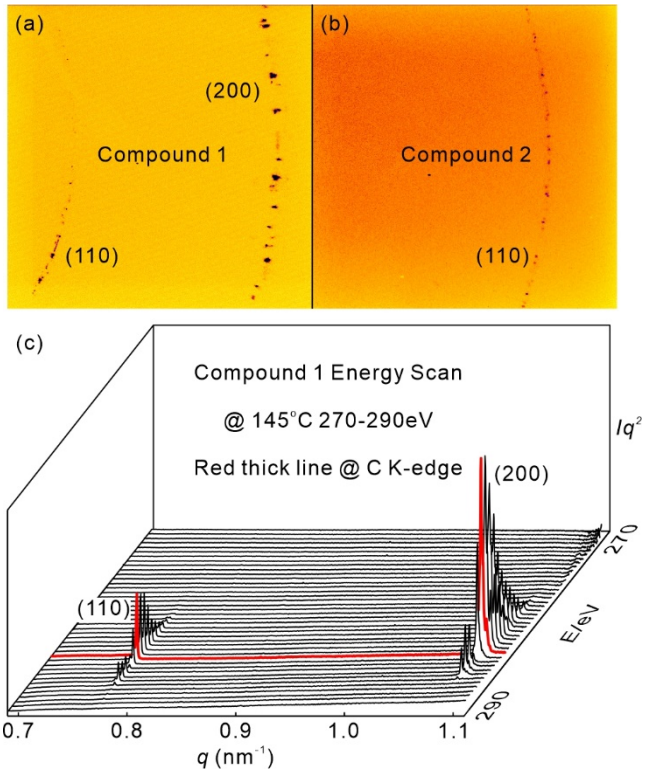

FIG.2. CCD images of resonant peaks of (a) compound 1 and (b) compound 2 at the carbon K-edge absorption energy 284 eV. Two resonant peaks of compound 1, visible only in the vicinity of the absorption edge, can be indexed as (110) and (200). Compound 2 exclusively exhibits only one, the (110) resonant peak. (c) Energy scan of compound 1 from 270 to 290 eV in a step of 0.5 eV. Red thick line corresponds to the scattering at the energy of the C K-edge, E = 284 eV.

The electron density (ED) maps of all studied compounds (FIG. 3) were reconstructed using intensity signals (FIG. S1) measured by SAXS. For the reconstruction, both the magnitude and phase of the structure factors, corresponding to a given set of Miller indices are required (see the Supplementary Information). The magnitudes of the

structure factors were obtained from the signal intensities (as a square root of intensity), while the phases in the centrosymmetric structures were assumed to be 0 or π. The phases of the two strongest peaks, (211) and (220), should be the same as shown using theoretical modelling [37] as well as by a direct reconstruction of the ED maps by using all possible combinations of phases. If both phases are π, the structure with the highest electron density inside the channels (Cub_{v2}) is obtained and if they both are 0, the situation is reversed, i.e, the electron density is lowest inside the channels (Cub_{v1}). We chose phases of the signals to be 0 for compound 2, and π for compounds 1 and 3, to ensure that the regions of high and low electron density in the reconstructed maps match the relative volumes of polar and nonpolar molecular parts.

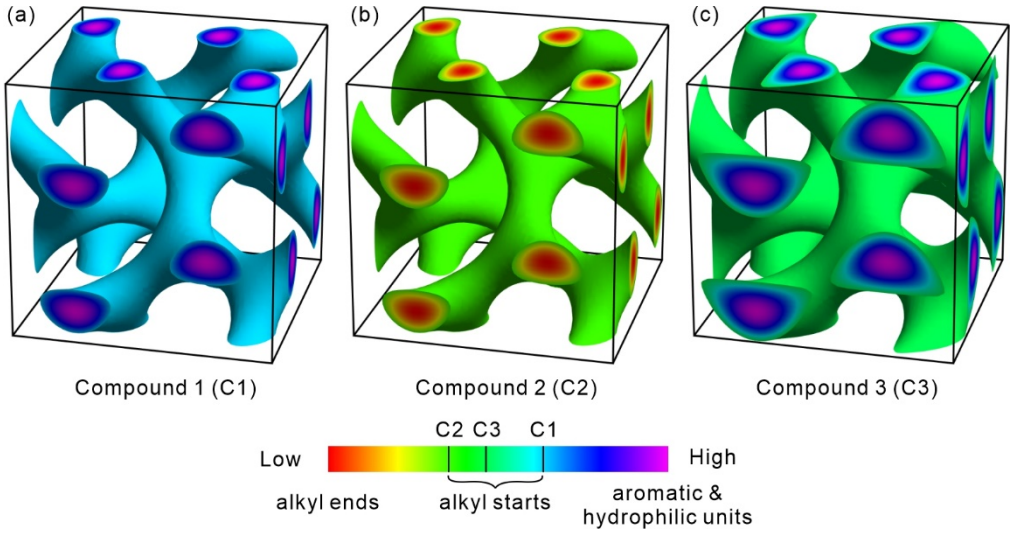

FIG.3. Reconstructed electron density maps of the $Ia\bar{3}d$ phase for (a) compound 1, (b) compound 2 and (c) compound 3. The color bar shows that a high electron density is in purple and low in red. The isoelectronic surfaces represent the boundaries between the aromatic cores and alkyl tails.

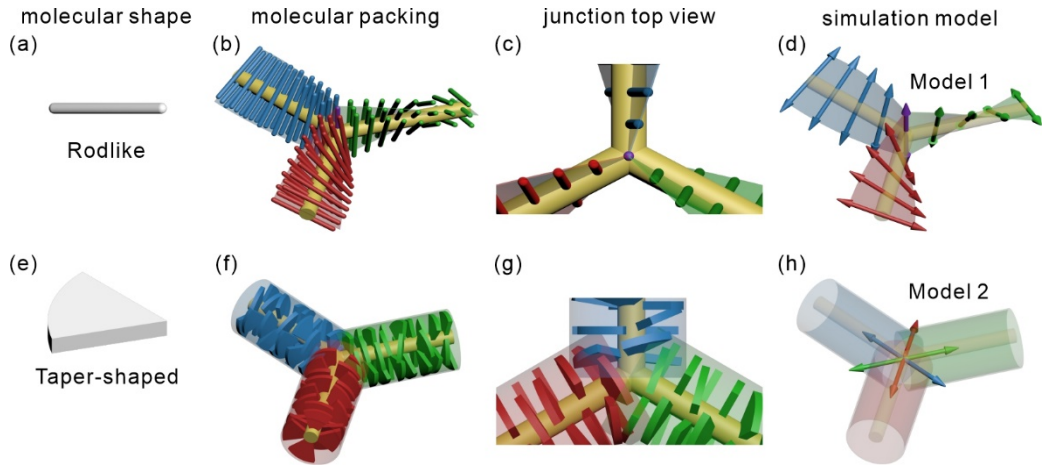

FIG.4. (a)-(d) Self-assembly of rodlike polycatenar molecules (compound 1) near the junctions of the gyroid networks: (a) schematic molecular shape; (b) proposed molecular packing near the three-way junction; (c) perfectly aligned junction (molecules from all three channels shown in different color transfer smoothly through the center of the junction without overlapping) and (d) simplified Model 1 used for simulation, where the arrows represent the polarizability axes. (e)-(h) Self-assembly of taper-shaped amphiphiles (compound 2): (e) schematic molecular shape; (f) proposed molecular packing near the three-way junction; (g) overlapping at the three-way junction leads to a mismatch and (h) simplified Model 2 used for simulation.

Next, we focus on the molecular orientation aspect in the proposed structure models. For compound 1 (FIG. 3a) the channels in the double gyroid network correspond to a high electron density region and are thus filled by aromatic cores. The molecular long axes are expected to be preferably parallel to each other and perpendicular to the channels, as shown in FIG. 4b, c. In this arrangement, the steric crowding leads to a helical twist along the gyroid networks, which is opposite in the two networks. Amphiphiles of compound 2 in the double gyroid phase (Fig. 3b) have the alkyl tails located in the channels. Four molecules per channel stratum are required to fill the space, as shown in FIG. 4f, g and Table S.IX. Filled by flexible alkyl tails, the channels are thus isotropic. Due to the taper molecular shape and the crowding of the polar end by three polar glycerol units, compound 2 could be assumed to give rise to a local helical organization around these alkyl chain channels, though such helical twist

would be expected to be significantly weaker than for compound 1 because of the reduced size of the aromatic core being insufficient to provide an efficient transmission of the helical twist. With such an order, there can be no smooth transfer of molecular order and helicity at the junctions. Such an organization is likely responsible for mismatch and discontinuity at the three-way junctions (FIG. 4g). For compound 3, the polar *N*-methyl glucamide tails occupying the double gyroid channels exhibit a similar isotropic feature as the alkyl chains in compound 2.. However, unlike compound 2, the two alkyl tails provide a reduced crowding of the periphery around the polar channels, thus reducing the driving force for a helical organization and this leads to the loss of any local helicity providing continuous and isotropic three-way junctions with randomized molecular packing in the columns and at the junctions.

Table I. Calculated tensor structure factor (F) and intensities (I) from models in FIG. 4

	Model 1	Model 2
$F_{(110)}$[a]	$f_{110}\begin{pmatrix} 0 & 1 & -1 \\ 1 & 0 & 0 \\ -1 & 0 & 0 \end{pmatrix}$	$f'_{110}\begin{pmatrix} 0 & 1 & -1 \\ 1 & 0 & 0 \\ -1 & 0 & 0 \end{pmatrix}$
$F_{(200)}$	$f_{200}\begin{pmatrix} 1 & 0 & 0 \\ 0 & -1 & 0 \\ 0 & 0 & 0 \end{pmatrix}$	0
Intensity[b]	$I(110) \propto 2f_{110}^2 \sin^2\theta$	
	$I(200) \propto f_{200}^2(\cos^2\alpha + \sin^4\theta \sin^2\alpha)$	

[a] f_{110} and f'_{110} represent different values from distinct models

[b] 2θ is the scattering angle and α the azimuthal angle

In order to obtain novel insights on molecular level packing from the RSoXS data, specifically the appearance of the forbidden peaks, we carried out model-dependent resonant X-ray scattering simulations. In Model 1, we considered anisotropic channels and continuous junctions (FIG. 4d). A stratum of rod-like molecules is replaced by

one resonant atom with the polarizability along the long molecular axis being different to the polarizability in the plane perpendicular to it. We name the axis, along which the polarizability in the Eigen frame of the atom differs from the polarizabilities along the other two axes as the "polarizability axis" (double-sided arrow in FIG. 4d). As molecular long axes rotate around the channel direction, so do the polarizability axes. At three-way junctions, the polarizability axis is perpendicular to the junction plane. In Model 2 we considered isotropic channels and mismatch junctions, which are modeled by three resonant atoms placed at the junction with their polarizability axes pointing along the three channels meeting at the junction (FIG. 4h). To predict the position and intensity of RSoXS peaks, we begin with the anisotropic polarizability of a resonant atom and assume that the tensor correction to the form factor is proportional to the anisotropic part of the polarizability tensor [38]. The structure tensor factor is then obtained by summing up the contributions from different resonant atoms (along the channels in Model 1 and in the junctions in Model 2), taking into account their position and orientation of the atoms' eigen coordinate systems with respect to the laboratory system. The polarization of incoming and scattered X-rays were also taken into consideration. The calculated results of structure factors and intensities are listed in Table I (see details of the calculation in the Supplementary information). The calculated positions and magnitudes of the non-zero tensor elements are in line with the $Ia\bar{3}d$ symmetry allowed terms [39, 40]. It is worth emphasizing that among the six models used for calculations (see supplementary for details), the appearance of the (200) peak arises from anisotropic channels (model 1) while the (110) peak arises from junctions (model 1 and model 2). In the calculated intensity, 2θ is the scattering angle and α the azimuthal angle, chosen in such a way that it is zero for the incident light being polarized in the direction perpendicular to the scattering plane (σ-polarization). The intensity of the (110) peak has no azimuthal dependence while the intensity of the (200) peak is largest for the σ-polarized incident and scattered light. Assuming the scattering angle is small and f_{110} and f_{200} are of the same order of magnitude, the modelling predicts that the intensity of the (110) peak is lower than the intensity of the (200) peak, which

is in line with the experimental results.

Comparison of experimental and simulation results (Fig. 5) revealed three specific molecular packing features of double gyroid phase. In the case of isotropic channels and mismatch of molecular orientation in the three-way junctions (model 2, Fig. 4), the model-dependent resonant X-ray scattering calculation predicted one resonant peak at (110), which indeed was observed in experiment for compound 2 (FIG. 5). Anisotropic packing of molecules along the channels (model 1, Fig. 4) is calculated to lead to two resonant peaks, (110) and (200) and these were observed for compound 1. The two widely accepted models of packing were thus proven to be valid. The absence of resonant peaks in compound 3 that has the ED map similar to compound 1, may be due to a combination of reduced molecular aspect ratio and reduced crowding at the periphery, thus rendering the local structure isotropic as well at the junctions as described above.

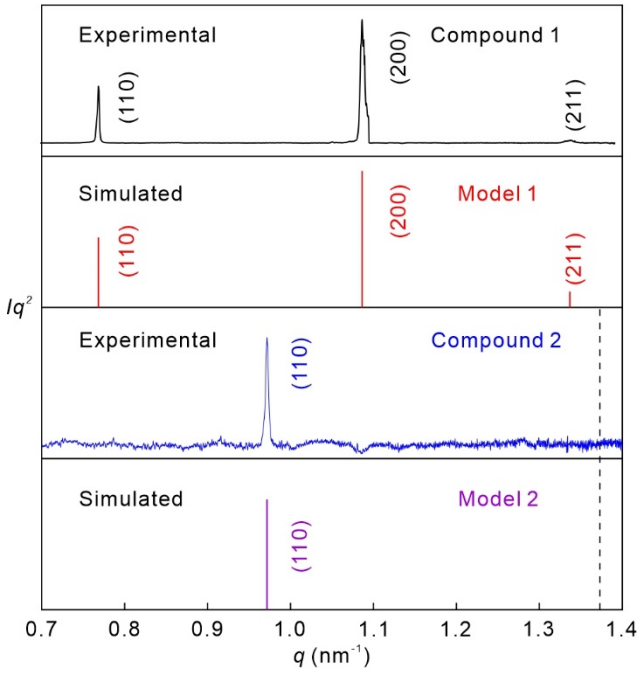

FIG.5. Comparison between the experimental RSoXS diffractograms and simulation results based on models shown in FIG. 4d (Model 1) and 4h (Model 2). Dashed line in Compound 2 and Model 2 marks the position of (200) peak if that peak was to exist experimentally. Note that the intensities of simulation result are not to scale.

To conclude, we have comparatively studied bicontinuous double gyroid cubic phases formed by rodlike polycatenar molecules as well as taper-shaped amphiphiles and revealed the local molecular packing in such a complex phase for the first time by employing a combination of RSoXS, SAXS and model-dependent resonant scattering pattern simulations. Clearly, such crystallographically forbidden peaks, which appear near elemental absorption edges, contain new structural information that can be used to reveal variations in molecular orientation in three-dimensional phases, for example, within a network of channels, beyond the electron density maps or morphology. As RSoXS can be tuned to specific bonds or elemental edges, it thus has a strong potential for distinguishing local orbital/bond/molecular packing modes in complex self-assembled structures. Despite a rather simplified theoretical calculation, a detailed description of the local molecular anisotropy is elucidated. This approach can potentially be made more robust by incorporating molecular orbitals, which can be calculated from density functional theory, in the polarizability tensor. Such comprehensive analysis will lead to a more precise understanding of molecular packing in complex materials, both man- or nature-made.

ACKNOWLEDGEMENT

We thank Dr. Cheng Wang, David Kilcoyne, Eric Schaible at ALS, LBNL for technical help at beamline 11.0.1.2 and 7.3.3. We acknowledge use of Beamlines 11.0.1.2 and 7.3.3 of the Advanced Light Source supported by the Director of the Office of Science, Office of Basic Energy Sciences, of the U.S. Department of Energy under contract no. DE-AC02-05CH11231. We are grateful to Beamline BL16B1 at SSRF (Shanghai Synchrotron Radiation Facility, China) for providing the beamtime. The work was also supported by National Natural Science Foundation of China (No. 21761132033 and 21774099), Science and Technology Agency of Shaanxi Province (No. 2016KW-050 and 2018KWZ-03). Y.C. also thanks China Scholarship Council (CSC) for providing financial support (201706280170) and ALS Doctoral Fellowship

in Residence Program. N.V. and E.G. acknowledge the support of the National Science Centre (Poland) under grant no. 2016/22/A/ST5/00319. N.V. acknowledges the support of the Slovenian Research Agency (ARRS), through the research core funding no. P1-0055. N.V. and E.G. thank professor Damian Pociecha for fruitful discussions. A. N. would like to acknowledge ALS Doctoral Fellowship in Residence Program and Eastman Chemical Company Fellowship for the financial support.

* Corresponding author

feng.liu@xjtu.edu.cn

† Corresponding author

Natasa.Vaupotic@um.si

‡ Corresponding author

chenhuizhu@lbl.gov

References

[1] V. Luzzati, Nature **217**, 1028 (1968).

[2] E. L. Thomas, D. B. Alward, D. J. Kinning, D. C. Martin, D. L. Handlin, and L. J. Fetters, Macromolecules **19**, 2197 (1986).

[3] Y. Fang, A. Levelut, and C. Destrade, Liq. Cryst. **7**, 265 (1990).

[4] M. Clerc and E. Dubois-Violette, J. Phys. II **4**, 275 (1994).

[5] J. M. Seddon and R. H. Templer, Philosophical Transactions: Physical Sciences and Engineering **344**, 377 (1993).

[6] K. Borisch, S. Diele, P. Göring, and C. Tschierske, Chem. Commun., 237 (1996).

[7] E. M. Landau and J. P. Rosenbusch, Proc. Natl Acad. Sci. USA **93**, 14532 (1996).

[8] G. Ungar, Y.-S. Liu, X.-B. Zeng, V. Percec, and W.-D. Cho, Science **299**, 1208 (2003).

[9] J.-F. Sadoc and J. Charvolin, Acta Crystallogr. Sect. A: Found. Crystallogr. **45**, 10 (1989).

[10] M. Impéror-Clerc, Curr. Opin. Colloid Interface Sci **9**, 370 (2005).

[11] M. Alaasar, S. Poppe, Q. Dong, F. Liu, and C. Tschierske, Chem. Commun. **52**, 13869 (2016).

[12] S. Poppe, C. Chen, F. Liu, and C. Tschierske, Chem. Commun. **54**, 11196 (2018).

[13] X. Zeng, S. Poppe, A. Lehmann, M. Prehm, C. Chen, F. Liu, H. Lu, G. Ungar, and C. Tschierske, Angew. Chem. Int. Ed. **58**, 7375 (2019).

[14] M. S. Morey, A. Davidson, and G. D. Stucky, J. Porous Mater. **5**, 195 (1998).

[15] M. Vallet-Regi, A. Rámila, R. P. del Real, and J. Pérez-Pariente, Chem. Mater. **13**, 308 (2001).

[16] T. Ichikawa, M. Yoshio, A. Hamasaki, T. Mukai, H. Ohno, and T. Kato, J. Am. Chem. Soc. **129**, 10662 (2007).

[17] M. A. Alam *et al.*, J. Am. Chem. Soc. **131**, 17722 (2009).

[18] E. J. W. Crossland *et al.*, Nano Lett. **9**, 2807 (2009).

[19] T. Ichikawa, T. Kato, and H. Ohno, J. Am. Chem. Soc. **134**, 11354 (2012).
[20] K. Borisch, S. Diele, P. Göring, H. Kresse, and C. Tschierske, J. Mater. Chem. **8**, 529 (1998).
[21] K. Borisch, C. Tschierske, P. Göring, and S. Diele, Langmuir **16**, 6701 (2000).
[22] C. Dressel, F. Liu, M. Prehm, X. Zeng, G. Ungar, and C. Tschierske, Angew. Chem. Int. Ed. **53**, 13115 (2014).
[23] V. Z.-H. Chan, J. Hoffman, V. Y. Lee, H. Iatrou, A. Avgeropoulos, N. Hadjichristidis, R. D. Miller, and E. L. Thomas, Science **286**, 1716 (1999).
[24] F. Liu, M. Prehm, X. Zeng, C. Tschierske, and G. Ungar, J. Am. Chem. Soc. **136**, 6846 (2014).
[25] R. H. Templer, Curr. Opin. Colloid Interface Sci **3**, 255 (1998).
[26] M. Poppe, C. Chen, F. Liu, S. Poppe, and C. Tschierske, Chem. Eur. J. **23**, 7196 (2017).
[27] P. Mach, R. Pindak, A. M. Levelut, P. Barois, H. T. Nguyen, C. C. Huang, and L. Furenlid, Phys. Rev. Lett. **81**, 1015 (1998).
[28] H. F. Gleeson and L. S. Hirst, ChemPhysChem **7**, 321 (2006).
[29] P. Fernandes, P. Barois, S. T. Wang, Z. Q. Liu, B. K. McCoy, C. C. Huang, R. Pindak, W. Caliebe, and H. T. Nguyen, Phys. Rev. Lett. **99**, 227801 (2007).
[30] C. L. Folcia *et al.*, Soft Matter **10**, 196 (2014).
[31] C. Zhu *et al.*, Nano Lett. **15**, 3420 (2015).
[32] C. Zhu *et al.*, Phys. Rev. Lett. **116**, 147803 (2016).
[33] J. M. Virgili, Y. Tao, J. B. Kortright, N. P. Balsara, and R. A. Segalman, Macromolecules **40**, 2092 (2007).
[34] J. R. Tumbleston, B. A. Collins, L. Yang, A. C. Stuart, E. Gann, W. Ma, W. You, and H. Ade, Nat. Photonics **8**, 385 (2014).
[35] M. Alaasar, M. Prehm, Y. Cao, F. Liu, and C. Tschierske, Angew. Chem. Int. Ed. **55**, 312 (2016).
[36] M. Alaasar, S. Poppe, Q. Dong, F. Liu, and C. Tschierske, Angew. Chem. Int. Ed. **56**, 10801 (2017).
[37] M. Vogrin, N. Vaupotič, M. Wojcik, J. Mieczkowski, K. Madrak, D. Pociecha, and E. Gorecka, Phys. Chem. Chem. Phys. **16**, 16067 (2014).
[38] A.-M. Levelut and B. Pansu, Phys. Rev. E: Stat. Nonlinear, Soft Matter Phys. **60**, 6803 (1999).
[39] V. Dmitrienko, Acta Crystallogr. Sect. A: Found. Crystallogr. **40**, 89 (1984).
[40] V. Dmitrienko, Acta Crystallogr. Sect. A: Found. Crystallogr. **39**, 29 (1983).